# Empirical Transfer Function Estimation with Differential Filtering and Its Application to Fine Positioning Control of Galvano Scanner

Yoshihiro Maeda, *Member*, and Makoto Iwasaki, *Fellow*

***Abstract*— Fast and precise point-to-point (PTP) positioning control is a critical technology for improving the throughput and product quality of industrial machines. This study aims to investigate the frequency response function (FRF) estimation method with differential filtering (ETFE-Diff: empirical transfer function estimation with differential filtering) that uses the input and output signals of PTP motion during processing operation and to apply ETFE-Diff to a feedforward (FF) compensation adjustment. In this study, the principle of ETFE-Diff for FRF estimation was clarified, compared to the existing FRF estimation methods, i.e., empirical transfer function estimation and local rational modeling. Moreover, the effectiveness of ETFE-Diff for FF compensation adjustment in improving positioning accuracy of a galvano scanner as an industrial servo system was experimentally demonstrated.**

***Index Terms*—Differential filtering, empirical transfer function estimation, frequency response function, leakage error, local rational modeling, point-to-point positioning control.**

## I. Introduction

Fast and precise point-to-point (PTP) positioning control is essential to maintain high throughput and product quality in many industrial machines such as electronics/semiconductor manufacturing machines, machine tools, and industrial robots [1]–[3]. In the design of a fine positioning control for the aforementioned industrial machines, frequency response function (FRF) is a basic and useful non-parametric model, and the estimation accuracy has a significant effect on the control performance [4]–[6]. However, during the processing operation, FRFs of servo mechanisms generally vary due to thermal effects, such as environmental temperature and self-heating of actuators [7]–[9].

Some FRF estimation methods that are effective for fine positioning control have been studied [10]–[13]. The most popular FRF estimation methods in industry are based on random/periodic noise excitation, multi-sine excitation, and sine sweep, and a plant FRF is estimated from the discrete Fourier transforms (DFTs) of measurable input and output signals of a plant based on the empirical transfer function estimation (ETFE) or spectral analysis [10], [14], [15]. In recent years, more powerful FRF estimation methods based on the local frequency modeling concept, such as local polynomial modeling (LPM) and local rational modeling (LRM), have been proposed [10], [12], [13]. These methods can achieve an accurate plant FRF by performing an experimental identification test using an additional excitation signal in the control system. Moreover, developmental studies for multi-input-multi-output and linear parameter varying systems have also been reported [16], [17]. However, as a trade-off, they are not favored during the processing operation because the additional excitation deteriorates the positioning accuracy. In contrast, other FRF estimation methods that estimate a plant FRF using measurable signals in a PTP positioning motion have been studied [18], [19], and these methods do not require additional excitation. However, an estimated FRF suffers from a leakage error because the DFTs of PTP motion signals generally include leakage effects owing to non-periodicity. A band-pass filter-based FRF estimation method has been presented in [20] to address the issue in FRF estimation. Furthermore, the differential filtering-based FRF estimation method (called "ETFE-Diff: empirical transfer function estimation with differential filtering" in this study) was proposed in [21], [22] to enable FRF estimation in short-time-interval PTP motions. Although the effectiveness of ETFE-Diff has been verified in the literature, the principle of leakage error suppression, that is, how a leakage error and a zero leakage error condition are mathematically formulated, has not yet been established. Additionally, the effectiveness of FRF estimation using PTP motion signals for designing a fine positioning control is yet to be clarified.

Therefore, this study investigates the FRF estimation principle of ETFE-Diff compared to ETFE as a classical method and LRM as an advanced method, and applies ETFE-Diff to design a fast and precise PTP positioning control. The contributions of this study are as follows.

1) The FRF estimation principle of ETFE-Diff, that is, a leakage error and a zero leakage error condition, was newly clarified via a theoretical analysis. Moreover, it was demonstrated via numerical experiments that ETFE-Diff can acquire an accurate FRF estimate when the zero leakage error condition holds in a PTP positioning

Manuscript received March 23, 2022; revised June 29, 2022; revised August 19; revised September 27, 2022; accepted October 12, 2022. This work was supported in part by Japan Society for the Promotion of Science (Grant number 20K04545), Nagamori Foundation, and ViaMechanics, Ltd.

Yoshihiro Maeda and Makoto Iwasaki are with the Electrical and Mechanical Engineering Program, the Department of Engineering, Nagoya Institute of Technology, Nagoya, 4668555, Japan (e-mail: ymaeda@nitech.ac.jp).

TABLE I
LIST OF ABBREVIATIONS.

| Abbreviation | Definition |
|---|---|
| FRF | Frequency Response Function |
| DFT | Discrete Fourier Transform |
| PTP | Point-To-Point |
| ETFE | Empirical Transfer Function Estimation |
| LPM | Local Polynomial Modeling |
| LRM | Local Rational Modeling |
| ETFE-Diff | Empirical Transfer Function Estimation with Differential Filtering |
| FF | Feedforward |
| FB | Feedback |
| DSP | Digital Signal Processor |

motion.

2) It was experimentally demonstrated that ETFE-Diff can precisely estimate the plant FRF and effectively adjust an FF compensation for variations in plant parameters owing to environmental temperature changes.

The above experiments were performed using a galvano scanner for printed circuit board laser processing machines as an example of an industrial servo system.

Table I lists the abbreviations used in this paper.

## II. FRF ESTIMATION USING PTP POSITIONING MOTION SIGNALS

In this section, the principles of FRF estimation of ETFE, LRM, and ETFE-Diff are explained, focusing on the leakage error [12], [13]. In particular, concerning ETFE-Diff, mathematical formulations of a leakage error and a zero leakage error condition are newly clarified as one of the significant contributions of this study.

### A. Problem Formulation

Consider a linear discrete-time single-input single-output system $P$ with input $u$ and output $y$ as shown in Fig. 1, where additional disturbing noises or nonlinear effects are neglected to simplify the discussion. The linear dynamics $P$ are described by the following $n$-th order state-space model:

$$\begin{aligned} \boldsymbol{x}_{\mathrm{p}}(t+1) &= \boldsymbol{A}_{\mathrm{p}}\boldsymbol{x}_{\mathrm{p}}(t) + \boldsymbol{B}_{\mathrm{p}}u(t) \\ y(t) &= \boldsymbol{C}_{\mathrm{p}}\boldsymbol{x}_{\mathrm{p}}(t) \end{aligned} \tag{1}$$

where $\boldsymbol{x}_{\mathrm{p}}(t)$ is the state vector at a discrete time $t$, and $\boldsymbol{A}_{\mathrm{p}}, \boldsymbol{B}_{\mathrm{p}}$, and $\boldsymbol{C}_{\mathrm{p}}$ are the state matrices. The $z$-domain transfer function of $P$ can be represented as

$$P(z) = \boldsymbol{C}_{\mathrm{p}}(z\boldsymbol{I} - \boldsymbol{A}_{\mathrm{p}})^{-1}\boldsymbol{B}_{\mathrm{p}} \tag{2}$$

The goal of the FRF estimation is to acquire an accurate estimate of the plant FRF of $P(z)$ from DFTs of the $N$-point finite-length signals $u(t)$ and $y(t)$ with $t = 0, 1, \ldots, N-1$ measured in a PTP positioning motion, as shown in Fig. 2. As a detailed problem statement, the following conditions should be noted.

C1: The input $u(t)$ and output $y(t)$ are non-periodic, that is, $\boldsymbol{x}_{\mathrm{p}}(0) \neq \boldsymbol{x}_{\mathrm{p}}(N)$.

C2: The plant is in a settled state at the start and end of the PTP positioning motion, that is, $\boldsymbol{x}_{\mathrm{p}}(t \leq -1) = \boldsymbol{x}_{\mathrm{p}}(0)$ and $\boldsymbol{x}_{\mathrm{p}}(t \geq N) = \boldsymbol{x}_{\mathrm{p}}(N-1)$.

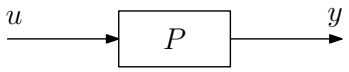


Fig. 1. Representation of simplified FRF estimation problem.

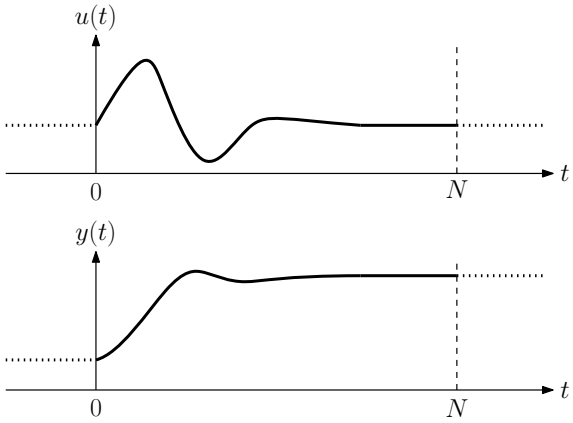


Fig. 2. Example waveforms of $u(t)$ and $y(t)$ in a PTP positioning motion.

C3: The input $u$ has a smooth frequency spectrum because the PTP positioning motion is performed without additional excitation.

In general, it is well known that C1 causes a leakage error in the DFT-based FRF estimation.

In this study, DFT of the $N$-point discrete-time signal $x(t)$ is defined as

$$X(k) = \sum_{t=0}^{N-1} x(t)e^{-j\frac{2\pi kt}{N}},\ k = 0, 1, \ldots, N-1 \tag{3}$$

where $k$ is the index corresponding to the frequency $\Omega_k = 2\pi k/(NT_{\mathrm{s}})$ with the sampling time $T_{\mathrm{s}}$.

### B. Emprical Transfer Function Estimation (ETFE)

ETFE is the simplest and most practical FRF estimation method based on DFT and is widely used in industrial applications [11], [14], [15]. From the state-space model of (1), the frequency-domain formulation of $y(t)$ is expressed as follows:

$$Y(k) = P(\Omega_k)U(k) + T(\Omega_k) \tag{4}$$

with

$$\begin{aligned} P(\Omega_k) &= \boldsymbol{C}_{\mathrm{p}}(e^{j\Omega_k T_{\mathrm{s}}}\boldsymbol{I} - \boldsymbol{A}_{\mathrm{p}})^{-1}\boldsymbol{B}_{\mathrm{p}} \\ T(\Omega_k) &= \boldsymbol{C}_{\mathrm{p}}(e^{j\Omega_k T_{\mathrm{s}}}\boldsymbol{I} - \boldsymbol{A}_{\mathrm{p}})^{-1}e^{j\Omega_k T_{\mathrm{s}}}\{\boldsymbol{x}_{\mathrm{p}}(0) - \boldsymbol{x}_{\mathrm{p}}(N)\} \end{aligned} \tag{5}$$

where $U(k)$ and $Y(k)$ are the DFTs of $u(t)$ and $y(t)$, respectively, $P(\Omega_k)$ is the plant FRF, and $T(\Omega_k)$ is the leakage error, which depends on the plant state vector $\boldsymbol{x}_{\mathrm{p}}(t)$ at $t = 0, N$. In the classical ETFE, the FRF estimate $\hat{P}_{\mathrm{ETFE}}(\Omega_k)$ is simply given by the ratio of $Y(k)$ and $U(k)$ as

$$\hat{P}_{\mathrm{ETFE}}(\Omega_k) := \frac{Y(k)}{U(k)} = P(\Omega_k) + \frac{T(\Omega_k)}{U(k)} \tag{6}$$

From (5), the zero leakage error condition under which $T(\Omega_k) = 0$ is derived as

$$\boldsymbol{x}_{\mathrm{p}}(0) = \boldsymbol{x}_{\mathrm{p}}(N) \tag{7}$$

As stated as C1 in II-A, because (7) does not hold in the PTP motion and hence $T(\Omega_k) \neq 0$, $\hat{P}_{\mathrm{ETFE}}(\Omega_k)$ clearly includes estimation errors.

### C. Local Rational Modeling (LRM)

LRM is an improved FRF estimation method that uses local parametric models with the simple assumption that the plant FRF $P(\Omega_k)$ and leakage error $T(\Omega_k)$ are closely related and can be approximated by smooth functions of frequency at local frequencies [13]. In LRM, $P(\Omega_k)$ and $T(\Omega_k)$ can be modeled for the local frequencies $k+w$ with $w = 0, \pm 1, \ldots, \pm N_{\mathrm{w}}$ as follows:

$$\begin{aligned} \tilde{P}(k+w) &= \frac{\tilde{N}_{\mathrm{P}}(k+w)}{\tilde{D}(k+w)} = \frac{\sum_{q=0}^{Q} \theta_{\mathrm{P}q}(k) w^q}{1 + \sum_{q=1}^{Q} \theta_{\mathrm{D}q}(k) w^q} \\ \tilde{T}(k+w) &= \frac{\tilde{N}_{\mathrm{T}}(k+w)}{\tilde{D}(k+w)} = \frac{\sum_{q=0}^{Q} \theta_{\mathrm{T}q}(k) w^q}{1 + \sum_{q=1}^{Q} \theta_{\mathrm{D}q}(k) w^q} \end{aligned} \tag{8}$$

where $\theta_{\mathrm{P}q}(k)$ is the numerator parameter of the plant FRF, $\theta_{\mathrm{T}q}(k)$ is the numerator parameter of the leakage error, $\theta_{\mathrm{D}q}(k)$ is the common denominator parameter, $w$ is the integer number used to define the local frequency window with a window size of $N_{\mathrm{w}}$, and $Q$ is the integer number defining the order of the polynomials. The parameters of the rational models can be obtained by solving the following linear least-squares problem:

$$\begin{aligned} \hat{\boldsymbol{\theta}}(k) = \arg\min_{\boldsymbol{\theta}(k)} \sum_{w=-N_{\mathrm{w}}}^{N_{\mathrm{w}}} \| &\tilde{D}(k+w) Y(k+w) \\ &- \tilde{N}_{\mathrm{P}}(k+w) U(k+w) - \tilde{N}_{\mathrm{T}}(k+w) \|^2 \end{aligned} \tag{9}$$

with

$$\begin{aligned} \boldsymbol{\theta}(k) = \{ &\theta_{\mathrm{P}0}(k), \ldots, \theta_{\mathrm{P}Q}(k), \theta_{\mathrm{T}0}(k), \ldots, \theta_{\mathrm{T}Q}(k), \\ &\theta_{\mathrm{D}1}(k), \ldots, \theta_{\mathrm{D}Q}(k) \} \end{aligned} \tag{10}$$

By solving (9) for $N$ frequencies, the FRF estimate $\hat{P}_{\mathrm{LRM}}(k)$ for $k = 0, 1, \ldots, N-1$ is determined as

$$\hat{P}_{\mathrm{LRM}}(k) := \tilde{P}(k+0) = \frac{\tilde{N}_{\mathrm{P}}(k+0)}{\tilde{D}(k+0)} = \hat{\theta}_{\mathrm{P}0}(k) \tag{11}$$

It is known that LRM can separately estimate $P(\Omega_k)$ and $T(\Omega_k)$ only when the input signal has a rough frequency spectrum [10]. However, in general, the input signal in a PTP positioning motion is not sufficiently rough in industrial servo systems, and additional excitation during processing operation is not favored because of deterioration of the positioning accuracy. Therefore, in this study, the LRM approach was directly applied to the PTP motion signals without additional excitation as stated as C3 in II-A to evaluate the FRF estimation ability. For more details of LRM and its application examples, see [10]–[13], [16], [17].

### D. ETFE with Differential Filtering (ETFE-Diff)

The FRF estimation with differential filtering presented in [21] can be interpreted as a type of ETFE because the FRF estimation approach is similar to ETFE (so it is called "ETFE with differential filtering" in this study). In this section, how a leakage error in ETFE-Diff is described by applying the differential filtering is clarified, compared to ETFE. Moreover, a zero leakage error condition in ETFE-Diff is theoretically derived.

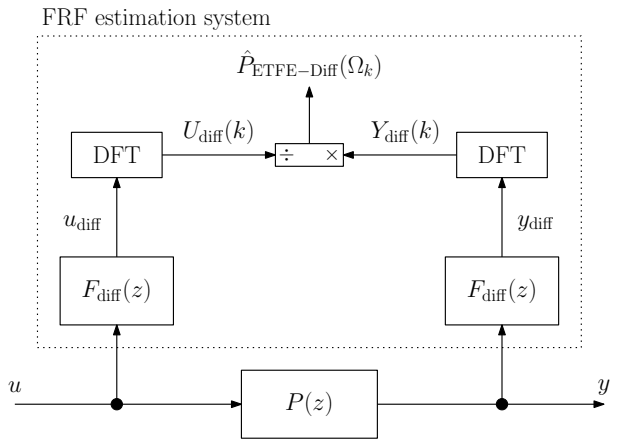


Fig. 3. Block diagram of FRF estimation system in ETFE-Diff.

Fig. 3 shows a block diagram of the FRF estimation system in ETFE-Diff, where "DFT" is the DFT calculation part, $\hat{P}_{\mathrm{ETFE-Diff}}(\Omega_k)$ is the plant FRF estimate, $F_{\mathrm{diff}}(z)$ is the differential filter $F_{\mathrm{diff}}(z) = 1 - z^{-1}$, $u_{\mathrm{diff}}$ is the filtered input, $y_{\mathrm{diff}}$ is the filtered output, $U_{\mathrm{diff}}(k)$ is the DFT of $u_{\mathrm{diff}}$, and $Y_{\mathrm{diff}}(k)$ is the DFT of $y_{\mathrm{diff}}$. In this system, first, the $N$-point time-domain difference signals $u_{\mathrm{diff}}(t)$ and $y_{\mathrm{diff}}(t)$ with $t = 0, 1, \ldots, N-1$ are calculated from the measured signals $u(t)$ and $y(t)$:

$$\begin{aligned} u_{\mathrm{diff}}(t) &= u(t) - u(t-1) \\ y_{\mathrm{diff}}(t) &= y(t) - y(t-1) \end{aligned} \tag{12}$$

Then, DFTs $U_{\mathrm{diff}}(k)$ and $Y_{\mathrm{diff}}(k)$ of (12) are calculated, and the FRF estimate $\hat{P}_{\mathrm{ETFE-Diff}}(\Omega_k)$ is determined by (13) as the ratio of $U_{\mathrm{diff}}(k)$ and $Y_{\mathrm{diff}}(k)$ in the same way as ETFE.

$$\hat{P}_{\mathrm{ETFE-Diff}}(\Omega_k) := \frac{Y_{\mathrm{diff}}(k)}{U_{\mathrm{diff}}(k)} \tag{13}$$

To clarify a leakage error in ETFE-Diff, the state-space expression of $F_{\mathrm{diff}}(z)$ for output is defined as

$$\begin{aligned} x_{\mathrm{f}}(t+1) &= y(t) \\ y_{\mathrm{diff}}(t) &= -x_{\mathrm{f}}(t) + y(t) \end{aligned} \tag{14}$$

By combining (1) and (14), the augmented system from $u(t)$ to $y_{\mathrm{diff}}(t)$ in Fig. 3 is formulated as follows:

$$\begin{aligned} \begin{bmatrix} \boldsymbol{x}_{\mathrm{p}}(t+1) \\ x_{\mathrm{f}}(t+1) \end{bmatrix} &= \begin{bmatrix} \boldsymbol{A}_{\mathrm{p}} & \boldsymbol{O} \\ \boldsymbol{C}_{\mathrm{p}} & 0 \end{bmatrix} \begin{bmatrix} \boldsymbol{x}_{\mathrm{p}}(t) \\ x_{\mathrm{f}}(t) \end{bmatrix} + \begin{bmatrix} \boldsymbol{B}_{\mathrm{p}} \\ 0 \end{bmatrix} u(t) \\ y_{\mathrm{diff}}(t) &= \begin{bmatrix} \boldsymbol{C}_{\mathrm{p}} & -1 \end{bmatrix} \begin{bmatrix} \boldsymbol{x}_{\mathrm{p}}(t) \\ x_{\mathrm{f}}(t) \end{bmatrix} \end{aligned} \tag{15}$$

In this case, the DFT $Y_{\mathrm{diff}}(k)$ is described as follows:

$$\begin{aligned} Y_{\mathrm{diff}}(k) = (1 - e^{-j\Omega_k T_{\mathrm{s}}}) &\{ P(\Omega_k) U(k) + T(\Omega_k) \} \\ &- \{ x_{\mathrm{f}}(0) - x_{\mathrm{f}}(N) \} \end{aligned} \tag{16}$$

Here, the DFT $U(k)$ is expressed by (17), considering $u_{\rm diff}(t) = u(t) - u(t-1)$.

$$\begin{aligned} U(k) &= \sum_{t=0}^{N-1} u(t) e^{-j\frac{2\pi kt}{N}} = \sum_{t=0}^{N-1} \{u(t-1) + u_{\rm diff}(t)\} e^{-j\frac{2\pi kt}{N}} \\ &= e^{-j\Omega_k T_{\rm s}} \sum_{t=0}^{N-1} u(t) e^{-j\frac{2\pi kt}{N}} + \sum_{t=0}^{N-1} u_{\rm diff}(t) e^{-j\frac{2\pi kt}{N}} \\ &\quad + u(-1) - u(N-1) \\ &= e^{-j\Omega_k T_{\rm s}} U(k) + U_{\rm diff}(k) + u(-1) - u(N-1) \end{aligned} \tag{17}$$

By organizing (17) for $U(k)$, the following equation can be obtained.

$$U(k) = (1 - e^{-j\Omega_k T_{\rm s}})^{-1} \{U_{\rm diff}(k) + u(-1) - u(N-1)\} \tag{18}$$

By substituting (18) to (16) and by expressing $u(\cdot)$ and $x_{\rm f}(\cdot)$ with $\boldsymbol{x}_{\rm p}(\cdot)$, $Y_{\rm diff}(k)$ is transformed as follows:

$$Y_{\rm diff}(k) = P(\Omega_k) U_{\rm diff}(k) + T_{\rm diff}(\Omega_k) \tag{19}$$

with

$$\begin{aligned} T_{\rm diff}(\Omega_k) = T(\Omega_k) - \boldsymbol{C}_{\rm p} (e^{j\Omega_k T_{\rm s}} \boldsymbol{I} - \boldsymbol{A}_{\rm p})^{-1} e^{j\Omega_k T_{\rm s}} \\ \{\boldsymbol{x}_{\rm p}(-1) - \boldsymbol{x}_{\rm p}(N-1)\} \end{aligned} \tag{20}$$

where $T_{\rm diff}(\Omega_k)$ is the leakage error in ETFE-Diff, which is expressed as the sum of the leakage error $T(\Omega_k)$ in ETFE and the additional term depending on the plant state vector $\boldsymbol{x}_{\rm p}(t)$ at $t = -1, N-1$. Hence, by applying the differential filtering to the measured input and output signals, the additional term changes the leakage error to be different from ETFE. From (19) and (20), the FRF estimate $\hat{P}_{\rm ETFE-Diff}(\Omega_k)$ of (13) is characterized by (21).

$$\hat{P}_{\rm ETFE-Diff}(\Omega_k) := \frac{Y_{\rm diff}(k)}{U_{\rm diff}(k)} = P(\Omega_k) + \frac{T_{\rm diff}(\Omega_k)}{U_{\rm diff}(k)} \tag{21}$$

Subsequently, to derive a zero leakage error condition in ETFE-Diff, $T_{\rm diff}(\Omega_k)$ of (20) is transformed as follows, considering $T(\Omega_k)$ and the additional term in (20) have similar structures:

$$\begin{aligned} T_{\rm diff}(\Omega_k) = \boldsymbol{C}_{\rm p} (e^{j\Omega_k T_{\rm s}} \boldsymbol{I} - \boldsymbol{A}_{\rm p})^{-1} e^{j\Omega_k T_{\rm s}} \\ [\{\boldsymbol{x}_{\rm p}(0) - \boldsymbol{x}_{\rm p}(N)\} - \{\boldsymbol{x}_{\rm p}(-1) - \boldsymbol{x}_{\rm p}(N-1)\}] \end{aligned} \tag{22}$$

From (22), the zero leakage error condition under which $T_{\rm diff}(\Omega_k) = 0$ is derived as

$$\boldsymbol{x}_{\rm p}(0) - \boldsymbol{x}_{\rm p}(N) = \boldsymbol{x}_{\rm p}(-1) - \boldsymbol{x}_{\rm p}(N-1) \tag{23}$$

Therefore, when the zero leakage error condition of (23) holds, the FRF estimate is consistent with the true plant FRF as

$$\hat{P}_{\rm ETFE-Diff}(\Omega_k) := \frac{Y_{\rm diff}(k)}{U_{\rm diff}(k)} = P(\Omega_k) \tag{24}$$

It is confirmed from the above theoretical analysis that applying the differential filtering changes the zero leakage error condition from $\boldsymbol{x}_{\rm p}(0) = \boldsymbol{x}_{\rm p}(N)$ in ETFE to $\boldsymbol{x}_{\rm p}(0) - \boldsymbol{x}_{\rm p}(N) = \boldsymbol{x}_{\rm p}(-1) - \boldsymbol{x}_{\rm p}(N-1)$. When the plant is in a settled state at the start and end of a PTP positioning motion as stated as C2 in II-A, (23) clearly holds and ETFE-Diff successfully suppresses the leakage error. In general, it is not difficult to measure such PTP motion signals during processing. Note that (23) is also valid for periodic motion (where $\boldsymbol{x}_{\rm p}(0) = \boldsymbol{x}_{\rm p}(N)$ and $\boldsymbol{x}_{\rm p}(-1) = \boldsymbol{x}_{\rm p}(N-1)$) and reciprocating motion (where $\boldsymbol{x}_{\rm p}(t \le 0) = \boldsymbol{x}_{\rm p}(t \ge N-1)$) as well as ETFE.

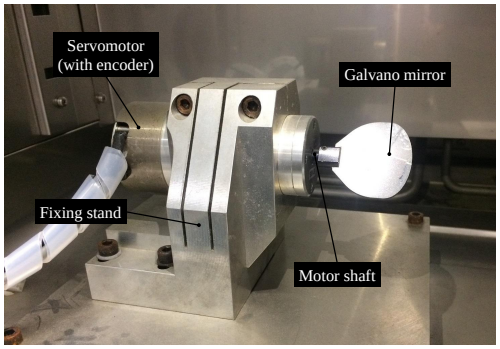


Fig. 4. External appearance of laboratory galvano scanner.

## III. Numerical Experiments of FRF Estimation

### A. Servo System

In this study, a galvano scanner, which is used as an industrial servo mechanism for positioning a laser beam in printed circuit board processing machines, is used as a target servo system. In laser processing machines, fast and precise PTP positioning control of a galvano scanner is crucial to improve the throughput and product quality. Fig. 4 shows the external appearance of a laboratory galvano scanner. A galvano mirror is rotated by a servomotor, and the motor angle is controlled by a servo controller mounted on a DSP (PDRS-6000, System Design Service). The motor angle was fed back to the DSP as a control output $y$ with a resolution of $1.49 \times 10^{-6}$ rad, and a motor current reference as a control input $u$ is calculated with a sampling time of $T_{\rm s} = 20$ $\mu$s in the DSP. The motor current was controlled via a servo amplifier. The galvano scanner was installed in a thermo-hygrostat chamber to vary the environmental temperature.

The red solid lines in Fig. 5 show the plant FRF of $y$ for $u$ measured using a sine sweep test at an environmental temperature of 25 °C as the default condition. The galvano scanner contains some resonance modes at high frequencies over 2 kHz, and the first and second resonance modes at 2.8 kHz and 6.1 kHz respectively, are attributed to the deformation of the galvano mirror and torsion of the motor shaft. For the following control design and numerical experiments, a linear dynamics model of the plant $P(s)$ is defined as (25) in the $s$-domain expression, considering the first and second resonance modes.

$$P(s) = \frac{K_{\rm t} K_{\rm a}}{J} \left( \frac{1}{s^2} + \sum_{i=1}^{2} \frac{k_i}{s^2 + 2\zeta_i \omega_i s + \omega_i^2} \right) e^{-Ls} \tag{25}$$

where $K_{\rm t}$ is the torque constant of the motor, $K_{\rm a}$ is the static gain of the servo amplifier, $J$ is the moment of inertia, $\omega_i$ is the natural angular frequency of the $i$-th resonance mode, $\zeta_i$ is the damping coefficient, $k_i$ is the resonance mode gain, and $L$ is the equivalent dead time for the phase delays of the

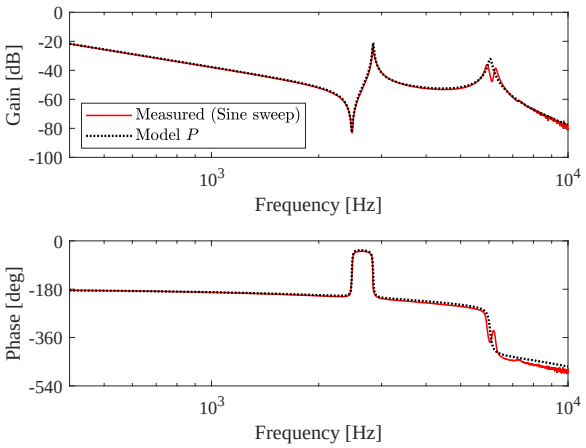


Fig. 5. Frequency characteristics of plant.

TABLE II
PARAMETERS OF PLANT MODEL $P(s)$.

| | | | |
|---|---|---|---|
| $K_\mathrm{t}$ [Nm/A] | $7.79\times10^{-2}$ | $K_\mathrm{a}$ | 0.333 |
| $J$ [kgm$^2$] | $1.43\times10^{-6}$ | $L$ [s] | $20.8\times10^{-6}$ |
| $\omega_1$ [rad/s] | $2\pi\times2842$ | $\omega_2$ [rad/s] | $2\pi\times6050$ |
| $\zeta_1$ | $3.80\times10^{-3}$ | $\zeta_2$ | $1.14\times10^{-2}$ |
| $k_1$ | 0.42 | $k_2$ | -1.60 |

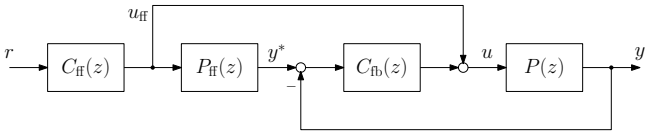


Fig. 6. Block diagram of two-degree-of-freedom position control system.

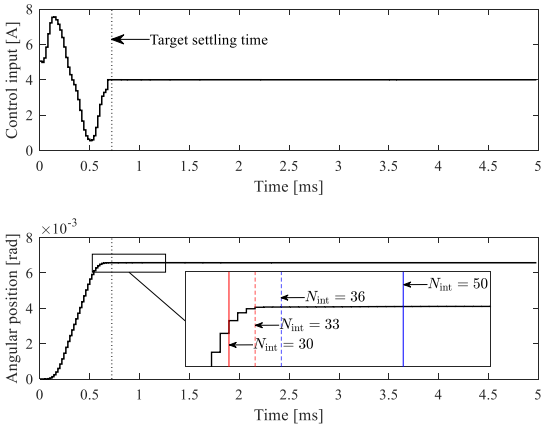


Fig. 7. Simulation waveforms of control input $u$ and angular position $y$ in a PTP positioning motion.

amplifier and D/A conversion. Table II lists the parameters of $P(s)$, while the black dotted lines in Fig. 5 show the FRF of $P(s)$ that accurately reproduces the measured FRF. Note that thermal effects, such as environmental temperature and self-heating, causes slight parameter variations in the galvano scanner, mainly in $K_\mathrm{t}$ and $\omega_1$, leading to a non-negligible deterioration in the positioning accuracy [8], [23]. Therefore, it is necessary to accurately identify parameters for $K_\mathrm{t}$ and $\omega_1$ is required to achieve fine positioning performance.

### B. Position Control System

Fig. 6 shows a block diagram of the two-degree-of-freedom position control system for the galvano scanner, where $P(z)$ is the discrete plant model of (25) with a zeroth-order hold, $P_\mathrm{ff}(z)$ is the plant model for generating the target position trajectory reference $y^*$, $C_\mathrm{fb}(z)$ is the feedback (FB) controller, $C_\mathrm{ff}(z)$ is the FF controller based on the deadbeat control manner [23], $r$ is the target position reference as a step input, and $u_\mathrm{ff}$ is the FF control input. $C_\mathrm{fb}(z)$ was constructed using a proportional-integral-derivative compensator and two second-order filters [24]. $C_\mathrm{ff}(z)$ is defined as

$$C_\mathrm{ff}(z)=\frac{a_{\mathrm{ff}M_\mathrm{ff}}z^{M_\mathrm{ff}}+a_{\mathrm{ff}(M_\mathrm{ff}-1)}z^{M_\mathrm{ff}-1}+\cdots+a_{\mathrm{ff}1}z+a_{\mathrm{ff}0}}{z^{M_\mathrm{ff}}} \tag{26}$$

where $a_{\mathrm{ff}m}$ with $m=0,1,\ldots,M_\mathrm{ff}$ are the free parameters. In the numerical experiments, $P_\mathrm{ff}(z)$ was set as $P_\mathrm{ff}(z)=P(z)$ and $C_\mathrm{ff}(z)$ was designed using the same model $P_\mathrm{ff}(z)$. Owing to FF compensation, the motor angular position $y$ precisely follows the reference $y^*$ while suppressing the vibratory responses of the resonance modes and realizing the deadbeat control property at $t\geq M_\mathrm{ff}$. In this study, the target control specifications were defined by considering a typical motion condition of the galvano scanner: target position of $r=6.58\times10^{-3}$ rad, target settling time of $0.72$ ms$(=36T_\mathrm{s})$, and target settling accuracy of $\pm1.97\times10^{-5}$ rad, and hence $M_\mathrm{ff}$ was set as $M_\mathrm{ff}=36$. For more details on the FF controller design, see [23].

### C. Comparisons of FRF Estimation Properties

First, the three FRF estimation methods, which are ETFE, LRM, and ETFE-Diff, were comparatively evaluated. The PTP positioning motion from a settled state, $\boldsymbol{x}_\mathrm{p}(0)=\boldsymbol{x}_\mathrm{p}(-1)=\boldsymbol{O}$, was performed using the control system depicted in Fig. 6, and the measured time-domain signals $u(t)$ and $y(t)$ with $N=8192$ shown in Fig. 7 were utilized to estimate the plant FRF. Herein, the plant sufficiently converges to a settled state by $t=N-1$, that is, $\boldsymbol{x}_\mathrm{p}(N)=\boldsymbol{x}_\mathrm{p}(N-1)$ holds. Clearly, $\boldsymbol{x}_\mathrm{p}(0)\neq\boldsymbol{x}_\mathrm{p}(N)$. In the simulations, disturbing noises and nonlinear effects, such as quantization, were not considered to evaluate the theoretical differences described in Section II, and the input frequency spectrum is smooth. In LRM, the local window size $N_\mathrm{w}$ and rational model order $Q$ were set as $N_\mathrm{w}=4$ and $Q=2$ respectively, with reference to [10]. ETFE and ETFE-Diff have no setting parameters.

Fig. 8 shows plant FRF estimates obtained by ETFE, LRM, and ETFE-Diff. Both ETFE (black solid) and LRM (red dash) include remarkable estimation errors owing to the leakage error in all frequency bands, which makes it difficult to accurately identify the rigid and resonance modes for the true FRF $P(\Omega_k)$ (black dot). Although LRM has a rational model-based separating capability to remove the leakage error, separating does not work effectively for such PTP positioning

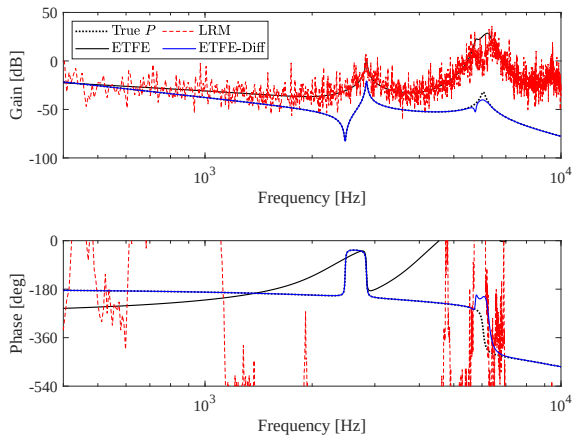


Fig. 8. Estimated FRFs for plant $P(\Omega_k)$.

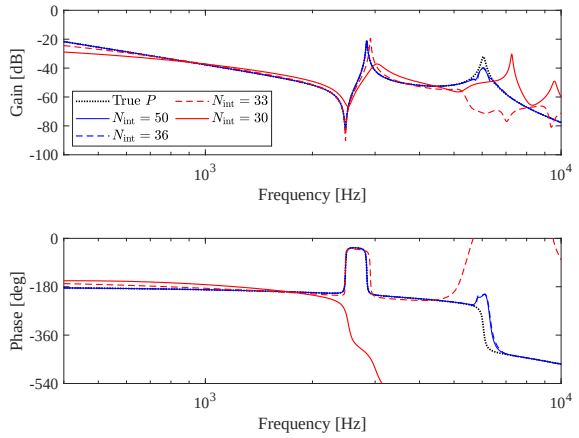


Fig. 9. Estimated FRFs by ETFE-Diff using different time interval signals.

motion signals without additional excitation. Consequently, it was difficult to further improve the estimation accuracy of LRM by changing $N_{\rm w}$ and $Q$. In contrast, ETFE-Diff (blue solid) significantly eliminates the leakage error by using a simple filtering approach, acquiring the most accurate FRF estimate.

Subsequently, regarding ETFE-Diff, the validity of zero leakage error condition of (23) was verified. From the response waveform of $y(t)$ near the target position shown in Fig. 7, it is confirmed that $y(t)$ almost converges to the settled state after the target settling time of $0.72\ \mathrm{ms} = 36T_{\rm s}$. Therefore, the time interval $N_{\rm int}$ of the measured signals for the FRF estimation was changed to $N_{\rm int} = 50, 36, 33$, and $30$ , while $\boldsymbol{x}_{\rm p}(N_{\rm int}) = \boldsymbol{x}_{\rm p}(N_{\rm int}-1)$ was required to hold (23). The measured $N_{\rm int}$-point signals were zero-padded after the end points to calculate the DFT with sufficient frequency resolution, and $N = 8192$-point signals were prepared in all cases. Fig. 9 shows the FRF estimates in the different time intervals. In the cases of $N_{\rm int} = 50$ (blue solid) and $N_{\rm int} = 36$ (blue dash), ETFE-Diff obtains accurate FRF

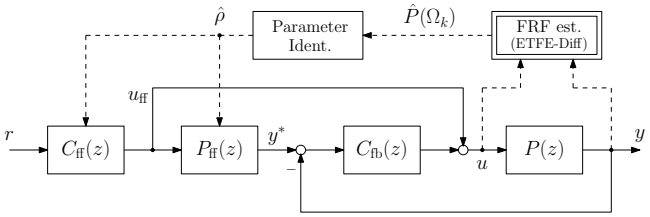


Fig. 10. Block diagram of two-degree-of-freedom position control system with FF compensation adjustment based on FRF estimation.

estimates because the plant sufficiently converges to the settled states: $\boldsymbol{x}_{\rm p}(N_{\rm int}) = \boldsymbol{x}_{\rm p}(N_{\rm int}-1)$. In contrast, in the cases of $N_{\rm int} = 33$ (red dash) and $N_{\rm int} = 30$ (red solid), the leakage error owing to the transient response in the settling motion, that is, $\boldsymbol{x}_{\rm p}(N_{\rm int}) \neq \boldsymbol{x}_{\rm p}(N_{\rm int}-1)$, deteriorated the estimation accuracy. The numerical experiments demonstrated that ETFE-Diff can successfully suppress the leakage error owing to the zero leakage error condition of (23) even with PTP positioning motion signals satisfying the conditions C1 $\sim$ C3 stated in II-A.

## IV. Experimental Evaluations of ETFE-Diff-Based FF Compensation Adjustment

The FRF estimation-based FF compensation adjustment system shown in Fig. 10 was constructed to evaluate the effectiveness of the ETFE-Diff-based FRF estimation in fine positioning control of the galvano scanner, compared to the case without the FF compensation adjustment shown in Fig. 6 as the default control method. First, the FRF estimation system calculates an plant FRF estimate $\hat{P}(\Omega_k)$ based on the ETFE-Diff using PTP motion signals $u(t)$ and $y(t)$. Subsequently, the torque constant and first resonance frequency are identified as $\hat{\boldsymbol{\rho}} = \{\hat{K}_{\rm t}, \hat{\omega}_1\}$, based on simple parameter identification algorithms. Thereafter, parameters of the FF controllers $C_{\rm ff}(z)$ and $P_{\rm ff}(z)$ are adjusted using $\hat{\boldsymbol{\rho}}$ based on the parameter adjustment method [23], and a PTP positioning motion is performed again. In the remainder of this section, the parameter identification algorithms and FF compensation adjustment method are briefly explained, and then the experimental results using the galvano scanner are presented.

### A. Parameter Identification Algorithms

In this study, simple and classical parameter identification algorithms that do not require complicated optimization techniques were employed considering practical use in the industry.

- Identification of $K_{\rm t}$
  The plant FRF at frequencies below the first resonance frequency can be approximated as $P(\Omega_k) = -K_{\rm t}K_{\rm a}/J\Omega_k^2$ considering only the rigid mode dynamics in (25). Thus, the torque constant is identified as $\hat{K}_{\rm t} = |\hat{P}(\Omega_k)|J\Omega_k^2/K_{\rm a}$ by using the FRF estimate $\hat{P}(\Omega_k)$. The final identification value for $\hat{K}_{\rm t}$ is acquired as the average in the frequency range of $2\pi \times [400, 1000]\ \mathrm{rad/s}$.
- Identification of $\omega_1$
  The identified value $\hat{\omega}_1$ for the first resonance frequency

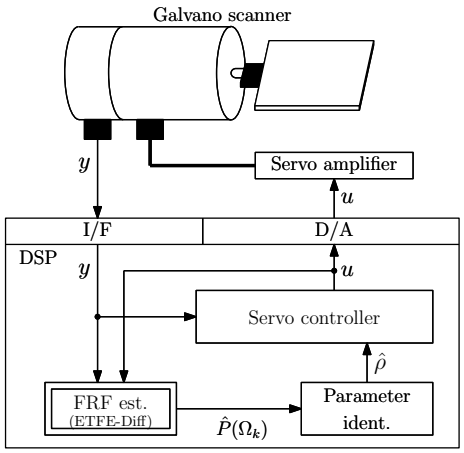


Fig. 11. Configuration of experimental setup of galvano scanner.

$\omega_1$ is simply defined as the frequency where $|\hat{P}(\Omega_k)|$ has the highest gain around the first resonance mode, by searching a narrow frequency window of $2\pi \times [2700, 2900]$ rad/s, including the resonance peak.

### B. FF Compensation Adjustment Method

The $z$-domain transfer function of the plant is defined as $P(z, \boldsymbol{\rho}) := N(z, \boldsymbol{\rho})/D(z, \boldsymbol{\rho})$ in terms of $\boldsymbol{\rho} = \{K_\mathrm{t}, \omega_1\}$. To achieve the deadbeat control property even with the parameter variation due to thermal effects, the FF controllers $C_\mathrm{ff}(z)$ and $P_\mathrm{ff}(z)$ are adjusted as follows, using the identified parameters $\hat{\boldsymbol{\rho}} = \{\hat{K}_\mathrm{t}, \hat{\omega}_1\}$ and the parameters $\hat{\boldsymbol{\rho}}_\mathrm{o}$ before adjusting:

$$\begin{aligned} C_\mathrm{ff}(z, \hat{\boldsymbol{\rho}}, \hat{\boldsymbol{\rho}}_\mathrm{o}) &:= \frac{N(1, \hat{\boldsymbol{\rho}}_\mathrm{o}) D(z, \hat{\boldsymbol{\rho}}) C_\mathrm{ffno}(z)}{N(1, \hat{\boldsymbol{\rho}}) z^{M_\mathrm{ff}}} \\ P_\mathrm{ff}(z, \hat{\boldsymbol{\rho}}) &:= \frac{N(z, \hat{\boldsymbol{\rho}})}{D(z, \hat{\boldsymbol{\rho}})} \end{aligned} \tag{27}$$

where $C_\mathrm{ffno}(z)$ is the fixed polynomial that is not adjusted in $C_\mathrm{ff}(z)$ [23]. By applying the above adjustments, if $\hat{\boldsymbol{\rho}} = \boldsymbol{\rho}$ holds, the control output obtained by the FF compensation can be characterized as follows:

$$Y(z) = \frac{N(1, \hat{\boldsymbol{\rho}}_\mathrm{o}) N(z, \boldsymbol{\rho}) C_\mathrm{ffno}(z)}{N(1, \hat{\boldsymbol{\rho}}) z^{M_\mathrm{ff}}} R(z) = Y^*(z) \tag{28}$$

Note that $N(1, \hat{\boldsymbol{\rho}})$ in the denominator does not affect the transient property. For more details on the adjustment method, see [23].

### C. Experimental Setup

Fig. 11 shows a configuration of the experimental setup of the galvano scanner used for performing both the ETFE-Diff-based FRF estimation and FF compensation adjustment. The FRF estimation by ETFE-Diff and parameter identification explained in IV-A were performed using single PTP motion signals $u(t)$ and $y(t)$ obtained by the FF compensation with $\hat{\boldsymbol{\rho}}_\mathrm{o}$. Subsequently, the FF controllers $C_\mathrm{ff}(z)$ and $P_\mathrm{ff}(z)$ in the servo controller were adjusted using $\hat{\boldsymbol{\rho}}$, as explained in IV-B, and the next PTP motion was performed by the FF compensation with $\hat{\boldsymbol{\rho}}$. The FRF estimation, parameter identification, and FF compensation adjustment were performed online via the DSP.

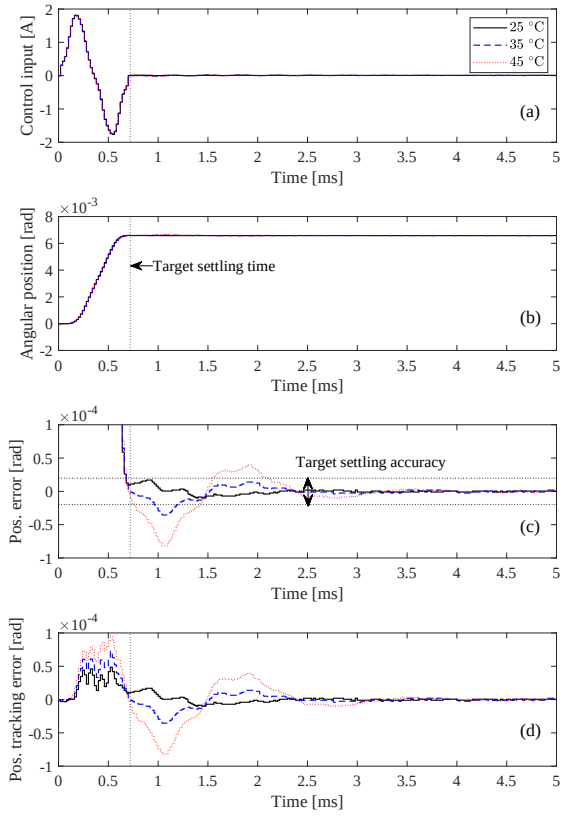


Fig. 12. Waveforms of PTP positioning responses before adjusting FF compensation at varied temperatures: (a) control input $u$; (b) angular position $y$; (c) position error $r - y$; (d) position tracking error $y^* - y$.

### D. Experimental Evaluations

Experimental evaluations were performed via PTP positioning motions at environmental temperatures of $25, 35$, and $45$ °C. Each PTP motion was performed from a sufficiently settled initial condition, that is, $\boldsymbol{x}_\mathrm{p}(0) = \boldsymbol{x}_\mathrm{p}(-1)$. Hence, to satisfy (23) in ETFE-Diff, $\boldsymbol{x}_\mathrm{p}(N) = \boldsymbol{x}_\mathrm{p}(N-1)$ is required. In the experiment, the default FF controllers $C_\mathrm{ff}(z)$ and $P_\mathrm{ff}(z)$ were designed with the model parameters of 25 °C, as listed in Table II, and $\hat{\boldsymbol{\rho}}_\mathrm{o}$ were set as $\hat{\boldsymbol{\rho}}_\mathrm{o} = \{7.79 \times 10^{-2}\ \mathrm{Nm/A}, 2\pi \times 2842\ \mathrm{rad/s}\}$. Note that although disturbing noises and nonlinear effects exist in the experimental system, the direct FRF estimation approach was applied because their effects are small.

Fig. 12 shows the response waveforms of the galvano scanner before adjusting the FF compensation at the varied temperatures. Although the input and output signals were almost the same regardless of the temperature variations in the macro view, as shown in Figs. 12(a) and 12(b), the perturbed responses at 35 °C and 45 °C deteriorated the settling accuracy in a micro view, as shown in Figs. 12(c) and 12(d).

The plant FRF estimated by ETFE-Diff at 25 °C using $N = 8192$-point time-domain signals $u(t)$ and $y(t)$ are shown in Fig. 13. Here, the plant FRF measured by sine sweep (black dot) is shown as reference for the true FRF, while the FRF estimates by ETFE and LRM are also shown for

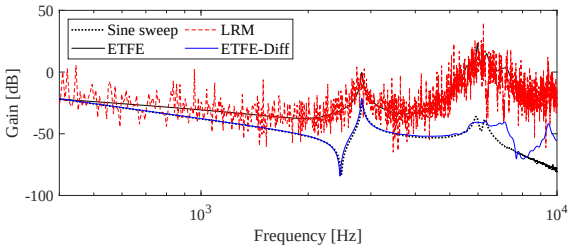


Fig. 13. Gain characteristics of estimated FRFs in experiment at 25 °C.

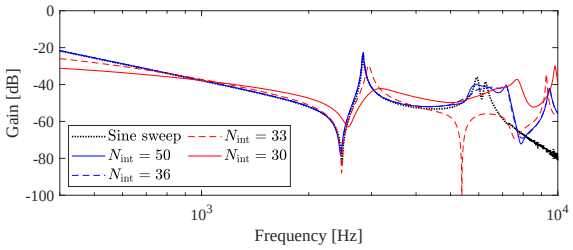


Fig. 14. Gain characteristics of estimated FRFs by ETFE-Diff using different time interval signals in experiment.

comparison. In the case of ETFE-Diff (blue solid), although frequency characteristics over 5 kHz could not be estimated clearly owing to the slight influence of disturbing noises and nonlinear effects, the most accurate FRF estimate was successfully acquired as in the numerical experiment in III-C. In contrast, both ETFE (black solid) and LRM (red dash) could not suppress the leakage error also in the experiment because of $\boldsymbol{x}_{\rm p}(0) \neq \boldsymbol{x}_{\rm p}(N)$ in ETFE and no additional excitation in LRM.

The FRF estimates using the measured signals at 25 °C with $N_{\rm int} = 50, 36, 33$, and 30 are shown in Fig. 14 to verify the validity of zero leakage error condition of (23) for the ETFE-Diff-based FRF estimation. For the FRF estimation, $N = 8192$-point time-domain signals with zero-padding were utilized in the same manner as in the numerical experiment of III-C. Although slight transient responses appear around the target position, the zero leakage error condition of (23) sufficiently holds after the target settling time of 0.72 ms$(= 36T_{\rm s})$. Consequently, accurate FRF estimates were acquired in the cases of $N_{\rm int} = 50, 36$.

Next, the estimated plant FRFs at varied temperatures are shown in Fig. 15 to clarify the effectiveness of the ETFE-Diff-based FF adjustment. In the experiment of FF adjustment, $N_{\rm int}$ was set as $N_{\rm int} = 50$, considering the time required for the transient responses at varied temperatures to sufficiently converge within the target settling accuracy, and $N = 32768$-point signals with zero-padding were utilized for FRF estimation with a sufficiently small frequency resolution of approximately 1.53 Hz. Except a frequency range over 5 kHz, ETFE-Diff acquired the FRF estimates eliminating the leakage error at varied temperatures, as shown in Fig. 15(a). In addition, the FRF estimates represent the variations in the rigid and first resonance modes owing to the environmental temperature, as shown in Figs. 15(b) and 15(c). From the estimated FRFs, $\hat{\boldsymbol{\rho}} = \{\hat{K}_{\rm t}, \hat{\omega}_1\}$ were identified, as listed in Table III. It was

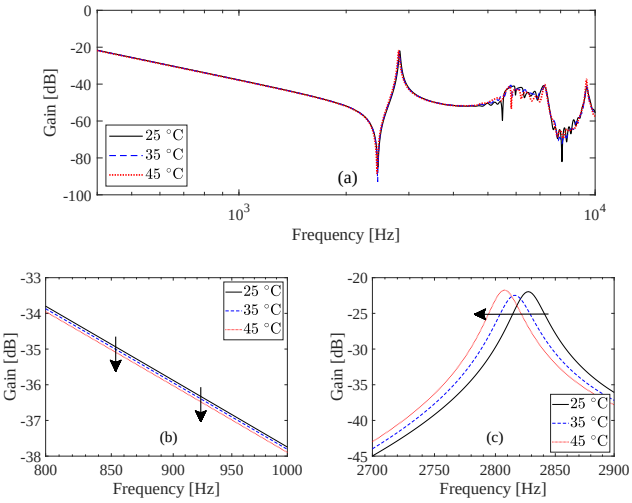


Fig. 15. Gain characteristics of FRF estimates before adjusting FF compensation at varied temperatures: (a) overview; (b) magnified view around rigid mode; (c) magnified view around first resonance mode.

TABLE III
IDENTIFIED PARAMETERS FROM FRFS ESTIMATED BY ETFE-DIFF.

| Parameter | Temperature [°C] | | |
|---|---|---|---|
| | 25 | 35 | 45 |
| $\hat{K}_{\rm t}$ [Nm/A] | $7.79\times10^{-2}$ | $7.72\times10^{-2}$ | $7.64\times10^{-2}$ |
| $\hat{\omega}_1$ [rad/s] | $2\pi\times2827$ | $2\pi\times2817$ | $2\pi\times2808$ |

confirmed that both $\hat{K}_{\rm t}$ and $\hat{\omega}_1$ decreased slightly when the temperature increased, which was the same trend as measured by sine sweep.

Fig. 16 shows the experimental PTP positioning responses at various temperatures after adjusting the FF compensation by $\hat{\boldsymbol{\rho}} = \{\hat{K}_{\rm t}, \hat{\omega}_1\}$. The adjusted FF compensation successfully suppressed the perturbed responses, resulting in fine positioning performance that satisfied a target settling accuracy of $\pm 1.97 \times 10^{-5}$ rad. The settling time, RMS of the position tracking error $y^* - y$, and maximum absolute value of the position error $r - y$ after the target settling time are summarized in Table IV, and compared to the values before adjusting the FF compensation. Before adjusting the FF compensation, the position tracking error and position error significantly increased owing to the thermal effect, and the settling time deteriorated to a maximum of 2.1 ms, which failed to satisfy the target time of 0.72 ms. In contrast, after adjusting the FF compensation, there was no deterioration in the settling time despite the varied temperatures, and the settling time was reduced by up to 69 % compared to that before adjusting the FF compensation.

## V. CONCLUSIONS

The ETFE-Diff-based FRF estimation and FF compensation adjustment are presented to realize fine PTP positioning performance, even if the plant parameters vary owing to thermal effects during the processing operation. Regarding the FRF estimation, the principle of ETFE-Diff to eliminate the leakage error was newly clarified, and compared to ETFE and LRM.

TABLE IV
COMPARISON OF POSITIONING PERFORMANCE AT VARIED TEMPERATURES.

| Temperature [°C] | Settling time [ms] | | RMS of pos. tracking error [$\mu$rad] | | Max. pos. error (absolute) [$\mu$rad] | |
|---|---|---|---|---|---|---|
| | Before FF adj. | After FF adj. | Before FF adj. | After FF adj. | Before FF adj. | After FF adj. |
| 25 | 0.68 | 0.66 | 10.80 | 6.15 | 16.96 | 6.55 |
| 35 | 1.20 | 0.66 | 17.64 | 6.93 | 35.47 | 7.06 |
| 45 | 2.10 | 0.66 | 30.82 | 7.24 | 81.93 | 10.03 |

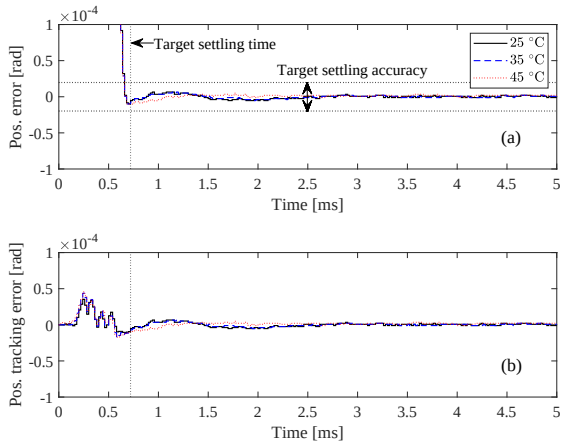


Fig. 16. Waveforms of PTP positioning responses after adjusting FF compensation at varied temperatures: (a) position error $r-y$; (b) position tracking error $y^* - y$.

The ability of ETFE-Diff to accurately estimate plant FRF when the zero leakage error condition holds in the positioning motion was also verified via the theoretical analysis and numerical experiments. The effectiveness of the ETFE-Diff-based FRF estimation and FF compensation adjustment was demonstrated experimentally with fast and precise positioning control of the galvano scanner under the environmental temperature variations.

## REFERENCES


[1] J. Wu, Z. Xiong, K.-M. Lee, and H. Ding, "High-acceleration precision point-to-point motion control with look-ahead properties," *IEEE Trans. Ind. Electron.*, vol. 58, no. 9, pp. 4343–4352, 2011.

[2] M. Hirata and F. Ueno, "Final-state control using polynomial and time-series data," *IEEE Trans. Magn.*, vol. 47, no. 7, pp. 1944–1950, 2011.

[3] M. Iwasaki, K. Seki, and Y. Maeda, "High-precision motion control techniques – A promising approach to improving motion performance," *IEEE Ind. Electron. Mag.*, vol. 6, no. 1, pp. 32–40, 2012.

[4] C.K. Pang and F.L. Lewis, "System identification of modal parameters in dual-stage Hard Disk Drives," in *Proc. 2009 IEEE Int. Conf. Control and Automation*, pp. 603–608, 2018.

[5] Y. Maeda, K. Harata, and M. Iwasaki, "A friction model-based frequency response analysis for frictional servo systems," *IEEE Trans. Ind. Informat.*, vol. 14, no. 11, pp. 5246–5255, 2018.

[6] R. de Rozario, A. Fleming, and T. Oomen, "Finite-time learning control using frequency response data with application to a nanopositioning stage," *IEEE/ASME Trans. Mechatron.*, vol. 24, no. 5, pp. 2085–2096, 2019.

[7] S. Nakagawa, M. Kobayashi, and T. Yamaguchi, "A higher bandwidth servo design with strain feedback control for magnetic disk drives," in *Proc. 2003 American Contr. Conf.*, vol. 3, 2003.

[8] D. Matsuka, T. Tanaka, and M. Iwasaki, "Thermal demagnetization compensation for fast and precise positioning in Galvanometer scanners," *IEEE Trans. Ind. Electron.*, vol. 63, no. 9, pp. 5514–5522, 2016.

[9] K. Sengchuai, B. Panyavoravaj, and N. Jindapetch, "Temperature effects on a simplified self-sensing actuation circuit for PZT micro-actuator in HDDs," *IEEE Sensors Journal*, vol. 19, no. 15, pp. 6205–6213, 2019.

[10] J. Schoukens, G. Vandersteen, K. Barbe, and R. Pintelon, "Non-parametric preprocessing in system identification: a powerful tool," in *Proc. European Control Conf. 2009*, pp. 1–14, 2009.

[11] J. Schoukens, K. Godfrey, and M. Schoukens, "Nonparametric data-driven modeling of linear systems," *IEEE Cont. Syst. Mag.*, Aug., pp. 49–88, 2018.

[12] R. Pintelon, J. Schoukens, and G. Vandersteen, "Frequency domain system identification using arbitrary signals," in *Proc. IEEE 35th Conf. Decision and Control*, pp. 2048–2051, 1996.

[13] T. McKelvey and G. Guerin, "Non-parametric frequency response estimation using a local rational model," in *Proc. 16th IFAC Symposium Syst. Ident.*, pp. 49–54, 2012.

[14] D.D.S. Mota, "Estimating the frequency response of an excitation system and synchronous motor: sinusoidal disturbances versus empirical transfer function estimate," *IEEE Power and Energy Technology Systems Journal*, vol. 5, no. 2, pp. 27–34, 2018.

[15] A. Mamatov and S. Lovlin, "Experimental estimation of frequency response functions of precision servo drive systems," in *Proc. 2018 X Int. Conf. Electrical Power Drive Syst.*, 2018.

[16] R. Voorhoeve, A. van der Maas, and T. Oomen, "Non-parametric identification of multivariable systems: A local rational modeling approach with application to a vibration isolation benchmark," *Mechanical Syst. Signal Processing*, vol. 105, May, pp. 129–152, 2018.

[17] R. van der Maas, A. van der Maas, R. Voorhoeve, and T. Oomen, "Accurate FRF identification of LPV systems: nD-LPM with application to a medical x-ray system," *IEEE Trans. Control Syst. Technology*, vol. 25, no. 5, pp. 1724–1735, 2017.

[18] Y. Matsui, H. Ayano, and K. Nakano, "Parametric plant modeling using one-shot closed-loop transient response data," in *Proc. 11th Int. Conf. Electrical Eng./Electron., Computer, Telecommunications Information Technology*, 2014.

[19] H. Sekine, S. Ueda, M. Suzuki, and M. Hirata, "System identification of a Galvano scanner using input-output data obtained from positioning control," in *Proc. 2015 European Control Conf.*, pp. 1297–1302, 2015.

[20] Y. Matsui, T. Kimura, and K. Nakano, "Plant model analysis based on closed-loop step response data," in *Proc. IEEE Int. Conf. Control Applications*, pp. 677–682, 2010.

[21] Y. Maeda, H. Tachibana, and M. Iwasaki, "Comparative evaluations of frequency response analysis methods for fast and precise point-to-point position control," in *Proc. 15th IEEE Int. Workshop Adv. Motion Control*, pp. 437–442, 2018.

[22] H. Tachibana, N. Tanaka, Y. Maeda, and M. Iwasaki, "Comparisons of frequency response function identification methods using single motion data: time- and frequency-domain approaches," in *Proc. 2019 IEEE Int. Conf. Mechatron.*, pp. 498–503, 2019.

[23] Y. Maeda and M. Iwasaki, "Improvement of adaptive property by adaptive deadbeat feedforward compensation without convex optimization," *IEEE Trans. Ind. Electron.*, vol. 62, no. 1, pp. 466–474, 2015.

[24] Y. Maeda, E. Kuroda, T. Uchizono, and M. Iwasaki, "Hybrid optimization method for high-performance cascade structure feedback controller design," in *Proc. 44th Annu. Conf. IEEE Ind. Electron. Society*, pp. 4588–4593, 2018.

**Yoshihiro Maeda** received the B.S., M.S., and Dr.Eng. degrees in electrical and computer engineering from Nagoya Institute of Technology (NITech), Nagoya, Japan, in 2004, 2006, and 2011, respectively. From 2008 to 2013, he was a Project Research Associate with Motion System Research Laboratory, NITech. Since 2015, he has been with NITech, where he is currently an Associate Professor with the Electrical and Mechanical Engineering Program, the Department of Engineering. He was with Denso, Ltd., Japan, from 2006 to 2007 and with Toyota Industries Corporation, Ltd., Japan, from 2013 to 2015. His research fields are autonomous control design and advanced motion control of mechatronic systems.

Dr. Maeda is a member of the Institute of Electrical Engineers of Japan and the Japan Society for Precision Engineering.

**Makoto Iwasaki** received the B.S., M.S., and Dr.Eng. degrees in electrical and computer engineering from Nagoya Institute of Technology (NITech), Nagoya, Japan, in 1986, 1988, and 1991, respectively. Since 1991, he has been with the Department of Computer Science and Engineering, NITech. He is currently a Professor with the Electrical and Mechanical Engineering Program, the Department of Engineering, NITech. His research interests include applications of motion control theory and soft computing techniques for motor/motion control.

Dr. Iwasaki is a member of the Institute of Electrical Engineers of Japan and the Japan Society for Precision Engineering.